Exploiting the information of the interferometric phase gradients. Examples and error characterization

Alessandro Parizzi, German Aerospace Agency (DLR), alessandro.parizzi@dlr.de, Germany
Wael Abdel Jaber, German Aerospace Agency (DLR), wael.abdeljaber@dlr.de, Germany

Abstract

SAR interferograms have been largely employed to estimate and interpret the motion of the Earth surface. The aim of this work is to provide a framework that allows the direct interpretation of DInSAR wrapped fringes for geophysical applications. Such measurements can be also be used to retrieve geophysical models parameters. An error analysis is discussed, then the methodology is demonstrated showing the estimation of strain and rotation components of a glacier flow and the inversion of an earthquake fault slips distribution using Okada dislocation model.

1 Introduction

This paper is aimed to discuss the use of interferometric phase gradients for geophysical applications. The work discusses two possible applications: the reconstruction of the 3D gradient tensor having different InSAR geometries and the inversion of the models parameters using gradients information. An analysis of the accuracy of the gradients estimation is then provided. Finally, in order to apply the framework on real data, two test cases have been considered. The study of ice deformation in a glacier flow and the inversion of earthquake fault slip using Okada dislocation model. These cases are particularly interesting because as far as the movement is quite big w.r.t the scale of interest it is possible to derive deformation measurements avoiding to resolve the phase ambiguities (phase unwrapping) [1] [2] [3].

2 Gradient Tensor from InSAR measurements

Considering a SAR interferogram, where all the topographic components have been compensated and neglecting the tropospheric delay, the expression of the absolute interferometric phase will be:

$$\phi = \frac{4\pi}{\lambda}\boldsymbol{\delta}\cdot\boldsymbol{s} \tag{1}$$

where λ is the wavelength. Being (e, n, v) the reference system oriented in accordance with the local east, the local north and the geodetic vertical, the change in radar range can be written as the projection of the displacement vector $\boldsymbol{\delta} = [\delta_e, \delta_n, \delta_v]$ on the sensing direction of the radar $\boldsymbol{s}$. In order to be able to separate the Strain and Rotation components the gradients tensor $\boldsymbol{\Psi}$ has to be estimated [4]. The gradient tensor $\boldsymbol{\Psi}$ represents the derivatives of $\boldsymbol{\delta} = [\delta_e, \delta_n, \delta_v]$. Since a single SAR interferometric pair is not able to provide resolution/sampling in the third dimension, it is not possible to collect information about the derivative w.r.t. the v axis. Therefore the third column of the gradient tensor can not be observed. For the sake of simplicity, the notation has been shortened to $u_{ij} = \partial\delta_i/\partial j$.

$$\boldsymbol{\Psi} = \left[\begin{array}{cc|c} u_{ee} & u_{en} & u_{ev} \\ u_{ne} & u_{nn} & u_{nv} \\ u_{ve} & u_{vn} & u_{vv} \end{array}\right] \tag{2}$$

Hence the displacement gradients observed in the sensing direction of the radar can be written as:

$$\vec{\nabla}(\boldsymbol{\delta}\cdot\boldsymbol{s}) = \boldsymbol{\Psi}^T\cdot\mathbf{s} = \frac{\lambda}{4\pi}\vec{\nabla}\phi \tag{3}$$

Equation (3) is a vector providing the derivatives of $\boldsymbol{\delta}\cdot\boldsymbol{s}$ w.r.t. the north and the east directions. Hence to retrieve the six components of $\boldsymbol{\Psi}$ at least three diverse interferometric measurements are needed.

2.1 Inversion of the Gradient Tensor

In Equation (3) the direct problem that links the phase gradients measurements with the gradient tensor $\boldsymbol{\Psi}$ has been defined. Let us now suppose in a general case to have N gradients measurements in N different geometries. Being $C_{d,k}$ the covariance matrix relative to the kth acquisition geometry, $\boldsymbol{\Psi}$ can be inverted in the Least Square sense by minimizing the figure of merit M w.r.t u_{ij}:

$$M = \sum_{k=0}^{N-1}\left(\frac{\lambda_k}{4\pi}\vec{\nabla}\phi_k - \boldsymbol{\Psi}(u_{ij})^T\cdot\mathbf{s}_k\right)^T C_{d,k}^{-1} \left(\frac{\lambda_k}{4\pi}\vec{\nabla}\phi_k - \boldsymbol{\Psi}(u_{ij})^T\cdot\mathbf{s}_k\right) \tag{4}$$

The inversion is completely analogous to the inversion of the 3D displacement vector [5] [6]. Therefore all the considerations regarding the performance with diverse acquisition geometries are valid also for the inversion of Equation (3).

2.2 Inversion of a set of model parameters from the Gradient Tensor

The paper discusses also the inversion of a set of model parameters $\boldsymbol{\xi}$ from interferometric gradient measurements. Let us now suppose to have a model of the surface motion described by a vector of parameters $\boldsymbol{\xi}$. $\boldsymbol{\Theta}(\boldsymbol{\xi})$ is the gradient tensor describing the gradients in function of the parameters to be estimated. Now analogously to Equation (4) it is possible to write a system of equation to be inverted w.r.t. the vector of parameters $\boldsymbol{\xi}$:

$$M = \sum_{k=0}^{N-1} \Big(\frac{\lambda_k}{4\pi} \vec{\nabla}\phi - \boldsymbol{\Theta}(\boldsymbol{\xi})^T \cdot \mathbf{s}_k \Big)^T C_{d,k}^{-1} \Big(\frac{\lambda_k}{4\pi} \vec{\nabla}\phi - \boldsymbol{\Theta}(\boldsymbol{\xi})^T \cdot \mathbf{s}_k \Big) \tag{5}$$

3 Phase Gradients estimation avoiding Phase Unwrapping

In the previous Section the general framework has been outlined. It is now necessary to discuss how the gradient measurements $\vec{\nabla}\phi_k$ can be estimated from the complex interferograms. Being (r, a) the range and azimuth coordinates in radar geometry, the interferogram is a complex number $z(r, a) = A(r, a) \exp\Big(j\phi(r, a)\Big)$ where A is the product of master and slave reflectivity and ϕ is the interferometric phase as in Equation (1). Considering the interferometric phase varying by several wavelengths within the scale of the deformation pattern, it is possible to perform a local linear approximation of the deformation phase. Hence in a given point r_0, a_0 the interferogram z can be substituted by its first order Taylor approximation:

$$z \approx Aexp\Big(j\frac{4\pi}{\lambda}\Big(\frac{\partial\delta_s}{\partial r}(r - r_0) + \frac{\partial\delta_s}{\partial a}(a - a_0)\Big) + \phi_0\Big) \tag{6}$$

where $\delta_s = \boldsymbol{\delta} \cdot \boldsymbol{s}$ is the projection of the displacement vector in line of sight. Equation (6) shows how the problem is basically the estimation of the main local fringe frequency of the interferogram. The problem can be solved in different ways with varying performance. Typically the periodogram estimator is used [7], however this estimator assumes flat spectrum which is not the case for the interferograms. Moreover in case of very strong fringe patterns, such an estimator does not take into account the spectral shift effect, hence reducing the estimation performance. In such a case the ML approach proposed in [8] would be more suitable. The inversions presented in the previous two sub-sections requires the knowledge of the error statistics of the equations. This allows to provide the optimal weighting of each equation. The main sources of error for the interferometric signals are the decorrelation and the delays coming from the propagation in the troposphere [9] and ionosphere.

3.1 Error in presence of white noise

The accuracy of the estimation of the local fringe frequency in a SAR interferogram are in general difficult to obtain in close form but they have to be computed numerically. An example is given in [8]. However if the fringe rate is not too high (low spectral shift) it is possible to approximate the interferogram as a complex sinusoid and the performance can be computed in close form as in [7].

3.2 Error in presence of spatially correlated noise

The additive delays generated by the propagation of the signal trough the troposphere generate a spatial phase pattern in SAR interferograms often named Atmospheric Phase Screen (APS). Such pattern can strongly vary according to the season, the time of the day and the atmospheric conditions. However its behavior can be good statistically described by a Covariance function $C_{APS}^{\phi}(r, a)$ if we assume the stationariety of the process [9]. The covariance function of the atmosphere gradients $C_{APS}^{\Delta}(r, a)$ knowing $C_{APS}^{\phi}(r, a)$ can be computed considering Fourier transform properties:

$$C_{APS}^{\Delta}(r, a) = -\frac{\partial^2 C_{APS}^{\phi}(r, a)}{\partial s^2} \tag{7}$$

where s is a generic direction along which the differentiation is carried out. This means also that even if $C_{APS}^{\phi}(r, a)$ has a circular symmetry such property will not be preserved in $C_{APS}^{\Delta}(r, a)$.

4 Strain And Rotation of a glacier flow: Example of Darwin Glacier

$\boldsymbol{\Psi}$ represents the first order Taylor approximation of the displacement field and it contains the information about all the relative movements of the portion of surface which it represents. The gradient tensor must be then decomposed in its symmetrical and anti-symmetrical parts. Those are respectively the strain $\boldsymbol{S}$ and rotation $\boldsymbol{R}$ components [4].

$$\begin{aligned} \boldsymbol{S} &= \frac{1}{2}(\boldsymbol{\Psi} + \boldsymbol{\Psi}^T) = \left[\begin{array}{cc|c} u_{ee} & \frac{u_{en}+u_{ne}}{2} & \frac{u_{ve}}{2} \\ \frac{u_{ne}+u_{en}}{2} & u_{nn} & \frac{u_{vn}}{2} \\ \hline \frac{u_{ve}}{2} & \frac{u_{vn}}{2} & 0 \end{array}\right] \\ \boldsymbol{R} &= \frac{1}{2}(\boldsymbol{\Psi} - \boldsymbol{\Psi}^T) = \left[\begin{array}{cc|c} 0 & \frac{u_{en}-u_{ne}}{2} & -\frac{u_{ve}}{2} \\ \frac{u_{ne}-u_{en}}{2} & 0 & -\frac{u_{vn}}{2} \\ \hline \frac{u_{ve}}{2} & \frac{u_{vn}}{2} & 0 \end{array}\right] \end{aligned} \tag{8}$$

As long as the derivatives w.r.t. the v direction (u_{ev}, u_{nv}, u_{vv}) are missing (see Equation (2)), only the 2×2 upper part of S and R tensors can be properly characterized . Consequently the third line and the third column of $\boldsymbol{S}$ and $\boldsymbol{R}$ end up being basically the same. This in practice means that even if the sensor is sensitive to

the gradients of the vertical motion, it will not be possible to resolve between a vertical tilt and a vertical extension/compression. Darwin Glacier ($79°53'S\ 159°00'E$) is an outlet glacier of the Transantarctic Mountains draining ice from the East Antarctic Ice Sheet into the Ross Ice Shelf. The strain $\boldsymbol{S}$ and rotation $\boldsymbol{R}$ components have been estimated using three available geometries (ascending right-looking, descending right-looking and descending left-looking). The temporal distribution of the acquisition is optimal since they have the minimal temporal baseline between the interferometric acquisitions, 11 days between the pairs and 1 day between the different geometries. Therefore the observed motion can be assumed to be the same. The components of the gradient tensor $\boldsymbol{\Psi}$ have then been inverted (Equation (4)) w.r.t. the geographic coordinates directions N/S and E/W and the tensors $\boldsymbol{S}$ and $\boldsymbol{R}$ have been computed as shown in Equation (8). In order to have a more intuitive measure unit the shear is displayed in [cm/km] and the rotation in [arcsec] (1 arcsec $\approx 0.0002°$). Results are shown in Figures 1.

5 Retrieve the Slip distribution of an earthquake: Example of Izmit earthquake

The Mw 7.6 Izmit earthquake occurred on the 17th August 1999. Because of the E/W orientation of the fault the co-seismic displacement was very well captured by ERS 1-2 SAR interferograms that show a dense pattern of azimuth oriented interferometric fringes. Since the high fringe density and the temporal decorrelation (35 days interferograms) make the phase unwrapping procedure particularly prone to errors, this case study fits very well a phase unwrapping-free approach. Equation (5) using a single geometry has been inverted in order to compute the slip distribution. In this case the parameter vector $\boldsymbol{\xi}$ represents the slips occurred along the fault plane. In order to carry out the inversion the fault plane has been divided in patches of 5x4 km that have been spatially regularized with a Laplacian operator inverting the equation system. The slip distribution has been inverted using the gradient information only. The estimated model seems to be able to explain most of the interferometric fringes Figure 2. Some residual is present in the central part probably due to the too simplified fault geometry and the reduced set of available data.

6 Discussion and Conclusions

This work gives a description of interferometric measurements not in terms of displacement but in terms of deformation/rotation of the observed surface. The idea is to extract LoS projected gradients information from the SAR interferograms and invert the displacement gradient tensor. From such a description is then possible to separate between gradients that are related with the surface deformation (strains) and the gradients that represent only a rotation. The methodology has been directly applied to the example of a glacier flow. The inversion of geophysical parameters using a model has been also implemented and tested on a real test case. The results look promising since the possibility of using interferometric phase gradients in slip distribution inversion was demonstrated. The integration of such measurements in studies of the coseismic displacement can provide information where the phase unwrapping cannot successfully work or integrate information coming from coregistration shifts.

References

[1] A. Sharov, "Gradient approach to insar modelling of glacial dynamics and morphology," *Proc. 22nd EARSeL Symp.*, vol. Millpress, Rotterdam, pp. 373–381, 2003.

[2] S. T. Ali and K. L. Feigl, "A new strategy for estimating geophysical parameters from insar data: Application to the kraf la central volcano in iceland," *Geochemistry, Geophysics and Geosystems*, vol. 16, no. 6, June 2012.

[3] A. Parizzi and M. Eineder, "Insar fringe frequency and deformation gradient: application for geophysical modelling." Presented at EGU General Assembly, Wien, 2015.

[4] C. J. V. der Veen, *Fundamentals of Glacier Dynamics*, T. . F. Group, Ed. CRC Press, 2013.

[5] T. J. Wright, B. E. Parsons, and Z. Lu, "Toward mapping surface deformation in three dimensions using insar," *Geophysical Research Letters*, vol. 31, 2004.

[6] H. Ansari, F. D. Zan, A. Parizzi, M. Eineder, K. Goel, and N. Adam, "Measuring 3-d surface motion with future sar systems based on reflector antennae," *IEEE Geoscience and Remote Sensing Letters*, vol. 13, no. 2, pp. 272–276, Feb 2016.

[7] S. Kay and R. Nekovei, "An efficient two-dimensional frequency estimator," *Acoustics, Speech and Signal Processing, IEEE Transactions on*, vol. 38, no. 10, pp. 1807–1809, Oct 1990.

[8] A. M. Guarnieri and S. Tebaldini, "Ml-based fringe-frequency estimation for insar," *IEEE Geoscience and Remote Sensing Letters*, vol. 7, no. 1, pp. 136–140, Jan 2010.

[9] R. Hanssen, *Radar Interferometry: Data Interpretation and Error Analysis*, Kluwer, Ed. Dordrecht, The Netherlands, 2001.

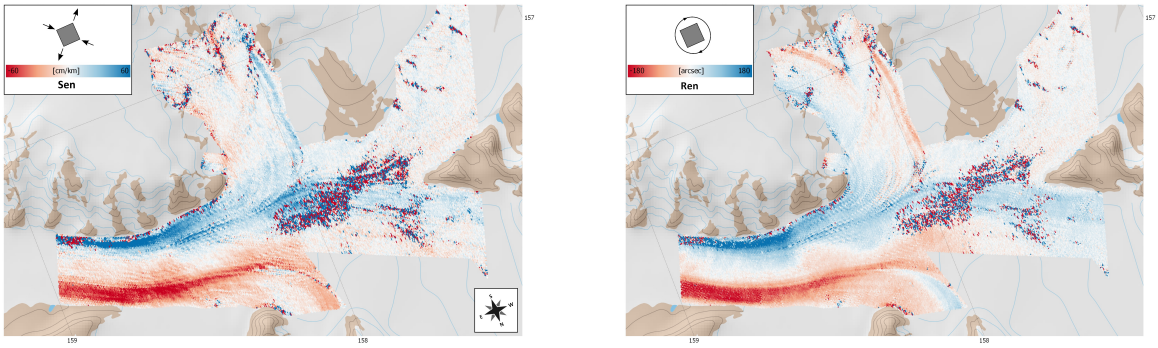

(a) **(b)**

Figure 1: Separation of the estimated gradient tensor in strain and rotation components. (a) shear component ($\boldsymbol{S}_{1,2}$) , (b) rotation component ($\boldsymbol{R}_{1,2}$)

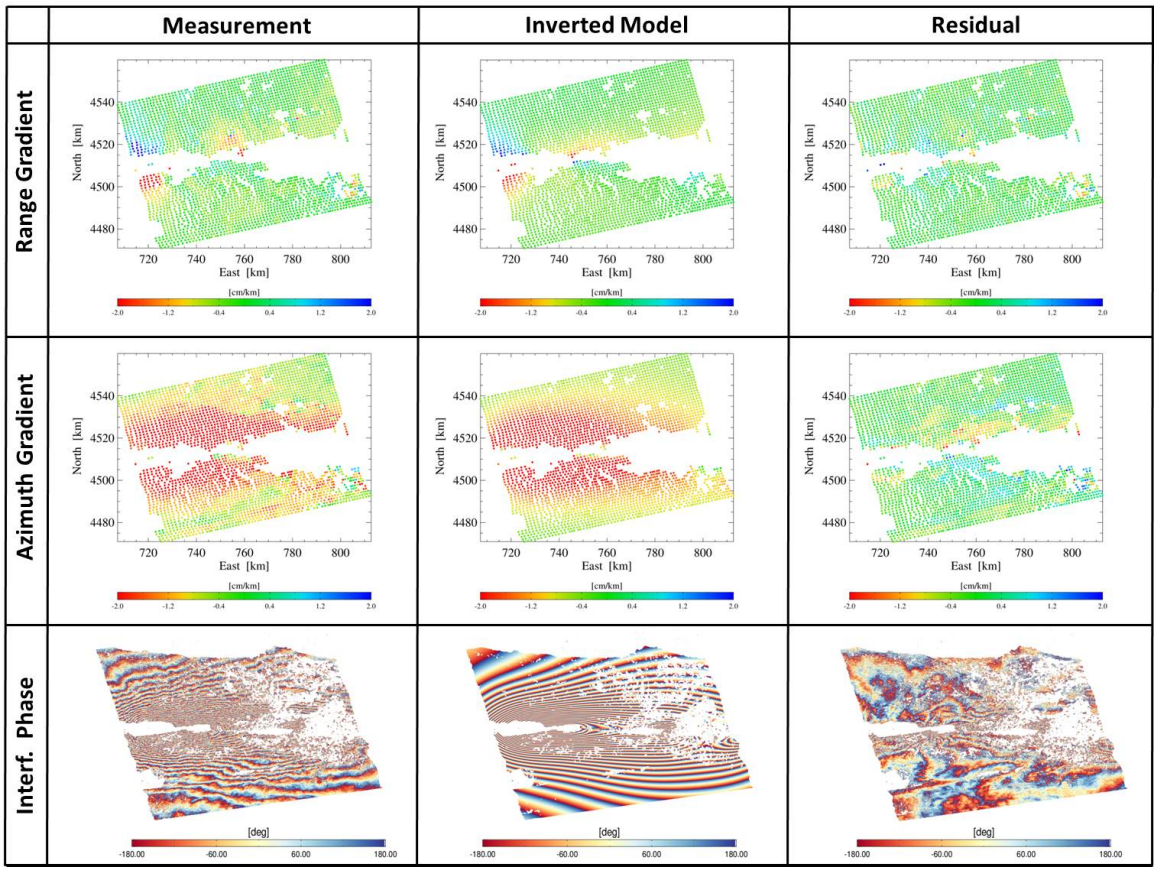

Figure 2: Measurements, inverted models and residuals for the Izmit test-case. The inversion has been performed using the gradients information only, interferometric phase is also shown in order to evaluate the accuracy of the estimation with a more sensitive indicator.